$PPQ_{10}PS_{300}$ cast from a 0.5 weight % solution have blue-shifted PL and PLE spectra with peaks at 437 and 388 nm, respectively (Fig. 5A), and the absorption band observed in the PLE is narrower. Time-resolved PL decay dynamics of the fluorescent PPQ blocks as isolated chains in PEO revealed two lifetimes [1.1 ns (30%) and 4.7 ns (70%)] compared with one lifetime (0.93 ns) (Fig. 5B) in the micellar films. This represents a large reduction in the excited state lifetime of PPQ chromophores in the microporous micellar films. Because the emission band is far removed from photonic band gaps of these microporous films, which are expected to be in the IR region, we rule out the large-scale periodic microstructure as the origin of the observed modification of photophysical properties. The decrease in lifetime is also the opposite of the predicted effect of a photonic crystal on spontaneous emission (*4*). H-Aggregation (*21*) of the PPQ blocks and hence the local structure of the micellar building blocks best explains the observed photophysical properties. H-Aggregation of the rigid rodlike blocks implies that they are orientationally aligned close to the radial direction in the spherical micellar assemblies (Fig. 1). Such an H-aggregation of conjugated molecules can lead to novel cooperative optical and nonlinear optical properties (*21*).

Because the size, mesostructure, and properties of micellar building blocks can be tailored through copolymer architecture and composition as well as the solution chemistry (*10*–*13*), we suggest that this hierarchical self-assembly approach is quite general for preparing periodic mesoporous polymeric materials. Besides photonic band gap materials and their associated applications (*4*), the ordered micellar films and their self-assembly process may have uses as models in tissue engineering and biomaterials (*22*), fabrication of molecular electronic devices (*23*), optically tunable and responsive coatings, and processing of "soft" colloidal materials. By combining different micellar building blocks and colloidal particles such as dendrimers or polymer lattices, self-assembly of very unusual periodic mesoscopic structures with tailorable functions may be possible.

References and Notes

1. C. T. Kresge, M. E. Leonowics, W. J. Roth, J. C. Vartuli, J. S. Beck, *Nature* **359**, 710 (1992); A. Sayari, *Chem. Mater.* **8**, 1840 (1996); Q. Huo, D. I. Margolese, G. D. Stucky, *ibid.*, p. 1147; D. Zhao *et al.*, *Science* **279**, 548 (1998); E. Krämer, S. Förster, C. Göltner, M. Antionetti, *Langmuir* **14**, 2027 (1998).
2. J. E. G. J. Wijnhoven and W. L. Vos, *Science* **281**, 802 (1998).
3. A. Imhor and D. J. Pine, *Nature* **389**, 948 (1997).
4. E. Yablonovitch, *J. Opt. Soc. Am. B* **10**, 283 (1993); J. D. Joannopoulos, P. R. Villeneuve, S. Fan, *Nature* **386**, 143 (1997); J. Martorell and N. M. Lawandy, *Phys. Rev. Lett.* **65**, 1877 (1990); H. Miguez *et al.*, *Appl. Phys. Lett.* **71**, 1148 (1997).
5. T. Bitzer, *Honeycomb Technology* (Chapman and Hall, London, 1997).
6. S. A. Jenekhe and X. L. Chen, *Science* **279**, 1903 (1998).
7. R. J. Hunter, *Foundations of Colloid Science*, vol. 1 (Clarendon, Oxford, UK, 1987); R. Buscall, T. Corner, J. F. Stagemen, Eds., *Polymer Colloids* (Elsevier, London, 1985); D. F. Evans and H. Wennerström, *The Colloidal Domain: Where Physics, Chemistry, Biology, and Technology Meet* (Wiley-VCH, New York, 1994).
8. A. Kose and S. J. Hachisu, *Colloid Interface Sci.* **46**, 460 (1974); S. Hachisu and S. Yoshimura, *Nature* **283**, 188 (1980); N. A. Clark, A. J. Hurd, B. J. Ackerson, *ibid.* **281**, 57 (1979); P. Pieranski, *Contemp. Phys.* **24**, 25 (1983); P. N. Pusey and W. van Megen, *Nature* **320**, 340 (1986); P. Bartlett, R. H. Ottewill, P. N. Pusey, *Phys. Rev. Lett.* **68**, 3801 (1992).
9. A. van Blaaderen, R. Ruel, P. Wiltzius, *Nature* **385**, 321 (1997); J. M. Weissman, H. B. Sunkara, A. S. Tse, S. A. Asher, *Science* **274**, 959 (1996).
10. G. A. McConnell, A. P. Gast, J. S. Huang, S. D. Smith, *Phys. Rev. Lett.* **71**, 2102 (1993); G. A. McConnell, M. Y. Lin, A. P. Gast, *Macromolecules* **28**, 6754 (1995); G. A. McConnell and A. P. Gast, *ibid.* **30**, 435 (1997); *Phys. Rev. E.* **54**, 5447 (1996).
11. S. E. Webber, P. Munk, Z. Tuzar, Eds., *Solvents and Self-Organization of Polymers* (Kluwer Academic, Dordrecht, 1996); S. E. Webber, *J. Phys. Chem. B* **102**, 2618 (1998); Z. Tuzar and P. Kratochvil, in *Surface and Colloid Science*, vol. 15, E. Matijevic, Ed. (Plenum, New York, 1993); pp. 1–83.
12. A. Halperin, M. Tirrell, T. P. Lodge, *Adv. Polymer Sci.* **100**, 31 (1992); S. Förster and M. Antonietti, *Adv. Mater.* **10**, 195 (1998); L. Zhang and A. Eisenberg, *J. Am. Chem. Soc.* **118**, 3168 (1996); *Science* **268**, 1728 (1995).
13. X. L. Chen and S. A Jenekhe, in preparation.
14. A. K. Agrawal and S. A. Jenekhe, *Macromolecules* **26**, 895 (1993); *Chem. Mater.* **8**, 579 (1996).
15. A. K. Agrawal, S. A. Jenekhe, H. Vanherzeele, J. S. Meth, *J. Phys. Chem.* **96**, 2837 (1992); S. A. Jenekhe *et al.*, *Chem. Mater.* **9**, 409 (1997).
16. J. A. Osaheni and S. A. Jenekhe, *J. Am. Chem. Soc.* **117**, 7389 (1995); S. A. Jenekhe and J. A. Osaheni, *Science* **265**, 765 (1994).
17. A. N. Semenov and S. V. Vasilenko, *Sov. Phys.* **63**, 70 (1986); A. N. Semenov, *Mol. Cryst. Liq. Cryst.* **209**, 191 (1991); A. Halperin, *Macromolecules* **23**, 2724 (1990); R. Holyst and M. Schick, *J. Chem. Phys.* **96**, 729 (1992); M. Müller and M. Schick, *Macromolecules* **29**, 8900 (1996); D. R. M. Williams and G. H. Fredrickson, *ibid.* **25**, 3561 (1992); D. R. M. Williams and A. Halperin, *Phys. Rev. Lett.* **71**, 1557 (1993); E. Raphael and G. P. de Gennes, *Physica A* **177**, 294 (1991); *Makromol. Chem. Macromol. Symp.* **62**, 1 (1992).
18. G. Widawski, M. Rawiso, B. Francois, *Nature* **369**, 387 (1994); B. Francois, O. Pitois, J. Francois, *Adv. Mater.* **7**, 1041 (1995). From a small-angle neutron-scattering study of poly(*p*-phenylene)-*block*-polystyrene in a selective solvent for PS, these authors have reported observation of spherical micelles of the conventional dense core-diffuse corona structure with a core diameter of 3 to 5 nm. These rod-coil diblocks and star homopolymers were reported to form ordered microporous films by an unclear phase separation mechanism. Our hierarchical self-assembly model of Fig. 1 can better explain the latter results but is inconsistent with their micellar structure.
19. Distinction between ABCABC- or ABABAB-type stacking of layers and hence whether the 3D lattice was fcc or hcp could not be established.
20. M. S. Dresselhaus, G. Dresselhaus, P. C. Eklund, *Science of Fullerenes and Carbon Nanotubes* (Academic Press, San Diego, CA, 1996).
21. M. Kasha, *Radiat. Res.* **20**, 55 (1963); R. M. Hochstrasser and M. Kasha, *Photochem. Photobiol.* **3**, 317 (1964); V. Czikkely, H. D. Försterling, H. Kuhn, *Chem. Phys.* **6**, 11 (1970); H. Chen, M. S. Farahat, K.-Y. Law, D. G. Whitten, *J. Am. Chem. Soc.* **118**, 2584 (1996).
22. J. H. Fendler, *Membrane Mimetic Chemistry* (Wiley, New York, 1982).
23. F. L. Carter, Ed., *Molecular Electronics II* (Marcel Dekker, New York, 1987).

24. This research was supported by the Office of Naval Research and in part by NSF (grants CTS-9311741 and CHE-9120001) and an Elon Huntington Hooker Fellowship to X.L.C.

30 September 1998; accepted 9 December 1998

Electron Transfer Between Bases in Double Helical DNA

Shana O. Kelley and Jacqueline K. Barton*

Fluorescent analogs of adenine that selectively oxidize guanine were used to investigate photoinduced electron transfer through the DNA π-stack as a function of reactant stacking and energetics. Small variations in these factors led to profound changes in the kinetics and distance dependences of DNA-mediated electron-transfer reactions. Values of β, a parameter reflecting the dependence of electron transfer on distance, ranged from 0.1 to 1.0 per angstrom. Strong stacking interactions result in the fastest electron-transfer kinetics. Electrons are thus transported preferentially through an intrastrand rather than interstrand pathway. Reactant energetics also modulate the distance dependence of DNA-mediated charge transport. These studies may resolve the range of disparate results previously reported, and paradigms must now be developed to describe these properties of the DNA π-stack, which can range from insulator- to "wire"-like.

The base pairs of the DNA double helix, an organized array of aromatic heterocycles, present a novel medium in which to explore π-stack–mediated electron transfer (ET) (*1*). Indeed, base damage and repair in DNA can be promoted across significant distances through long-range ET (*2*). However, experiments addressing ET through DNA using pendant donors and acceptors have provided remarkably different assessments of the electronic coupling provided by DNA (*3*–*10*).

Beckman Institute, Division of Chemistry and Chemical Engineering, California Institute of Technology, Pasadena, CA 91125, USA. jkbarton@cco.caltech.edu

*To whom correspondence should be addressed.

Values for β, the decay of electronic coupling with distance (*11*), ranging from ≤0.1 $Å^{-1}$ to 1.4 $Å^{-1}$ have been reported. Reactions using intercalating or well-stacked probes proceed on a fast time scale and exhibit shallow distance dependences (β ≤ 0.1 to 0.4 $Å^{-1}$) (*4–6*). Moreover, a profound sensitivity to stacking has been observed; in the presence of base mismatches or other stacking perturbations, long-range ET is essentially turned off (*4–6*). Other studies of donors and acceptors interacting with the DNA base stack through σ-linkages or limited stacking have revealed much slower ET kinetics and steeper distance dependences (β = 0.6 to 1.4 $Å^{-1}$) (*7–10*).

We have studied photoinduced ET between DNA bases incorporated within synthetic duplexes to evaluate ET through DNA directly without the structural ambiguity associated with pendant donors and acceptors. We present a systematic series of fluorescence quenching measurements within structurally well-characterized DNA assemblies that illustrate the large range of reactivity that results from subtle changes in the stacking or orientation of reactants within the helix. Moreover, we present results indicating that reactant energetics also affect the distance dependence of ET through DNA; these studies may provide an experimental demonstration of tunneling energy effects in DNA-mediated ET reactions.

The reactivity of two fluorescent analogs of adenine, 2-aminopurine (A_2) (*12*) and 1,N^6-ethenoadenine (A_ε) (*13*), with DNA nucleotides was first explored in quenching titrations in aqueous solution (see supplementary material available at www.sciencemag.org/feature/data/984892.shl). A_2 and A_ε both emit strongly from π-π* excited states not populated in the natural DNA bases (*14, 15*) (Scheme 1). The fluorescence of both of these bases is efficiently quenched by deazaguanine (Z) and guanine (G), with only small amounts of quenching observed with inosine (I) and the other DNA bases with significantly higher redox potentials (*16–19*). For A_2, Stern-Volmer quenching rate constants (k_q) of 2.2(4) × 10^9 $M^{-1}s^{-1}$ for guanosine triphosphate (GTP) and 5.2(3) × 10^9 $M^{-1}s^{-1}$ for ZTP were derived from these titrations. For A_ε and GTP, k_q = 1.9(2) × 10^9 $M^{-1}s^{-1}$, and for A_ε and ZTP, k_q = 4.6(4) × 10^9 $M^{-1}s^{-1}$(numbers in parentheses indicate standard errors in the last digit). Both fluorophores are quenched by these nucleotides in the order anticipated on the basis of the driving force (as deduced from oxidation potentials, E°) for ET ($E^\circ_{ZTP} < E^\circ_{GTP} < E^\circ_{ITP}$). Moreover, transient absorption studies provide strong evidence for charge-separated products in these photoinduced reactions (*20*). Along with the lack of spectral overlap between these donors and acceptors, these data support ET as the source of this fluorescence quenching. The similarity among the quenching constants obtained for these two different fluorescent bases shows that the reactions have comparable driving forces, consistent with the excited-state potentials for A_2 and A_ε calculated from electrochemical measurements and spectral properties (*21*).

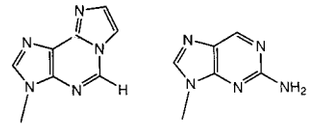

A_ε A_2

Scheme 1. Structure of fluorescent analogs of adenine, A_ε and A_2.

Having identified base analogs that undergo photoinduced ET reactions, we could prepare DNA assemblies through chemical synthesis in which the positions of donor and acceptors were known precisely and varied systematically. DNA-mediated photooxidations of G by A_2 and A_ε were therefore examined in a series of 12–base pair (bp) DNA duplexes at donor-acceptor separations of 3.4 to 13.6 Å. In the duplexes, the donor (G) and acceptor (A_2 or A_ε) were located on the same strand. The remaining heterogeneous sequences were composed of I-C and A-T pairs that do not react with photoexcited A_2 or A_ε (*22*).

Table 1. Steady-state quantum yields and quenching efficiencies for A_ε-G duplexes. Distances were calculated as in Fig. 3. Samples were prepared as in (*39*). Quantum yields (Φ) for 100 μM duplex samples in 100 mM phosphate (pH 7) were measured at 20°C relative to 100 μM A_εTP, Φ = 0.60 (*13*). All solutions exhibited identical absorbances. Steady-state fluorescence intensity measurements were made at 20°C unless otherwise specified on an SLM 8000 spectrofluorimeter or a ISS K2 spectrofluorimeter. Sample excitation was performed with λ_{exc} = 335 nm, and spectra were integrated from 355 to 525 nm. Normalized fluorescence spectra of quenched and unquenched samples were identical. All fraction quenched ($F_q = 1 - \Phi_G/\Phi_I$) values obtained from steady-state fluorescence measurements were calculated from four to six sets of samples and least three independent oligonucleotide syntheses. Numbers in parentheses represent standard deviation values.

Duplex	A_ε-Y distance (Å)	$\Phi_{Y=I}$	$\Phi_{Y=G}$	F_q
5′-TAIε**Y**ITITTATIA ATCTCCACAATACT	3.4	0.26 (4)	0.04 (2)	0.85 (7)
5′-TAIε**A**YITATTAIA ATCTTCCATAATCT	6.8	0.34 (4)	0.28 (4)	0.18 (4)
5′-TAIεAA**Y**ITITAIA ATCTTTCCACATCT	10.2	0.34 (5)	0.34 (4)	0.01 (1)

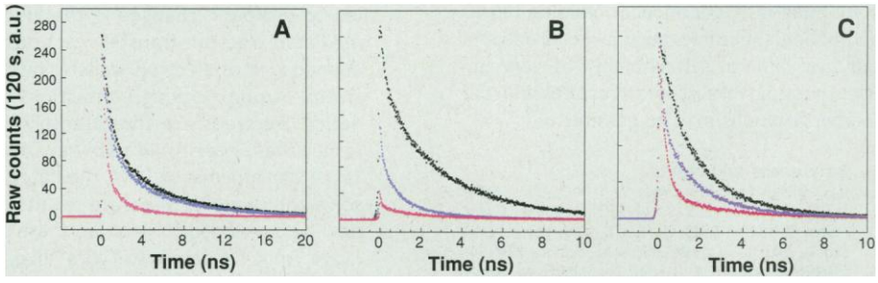

Fig. 1. Fluorescence decay profiles for A_ε and A_2 obtained by TCSPC; sets shown were obtained by collecting counts for 120 s under conditions of steady laser power (a.u., arbitrary units). Data shown in (**A**) for A_ε and (**B**) for A_2 (intrastrand reaction) correspond to A_ε-G or A_2-G separations of 3.4 Å (red) and 6.8 Å (blue) compared with an unquenched I-containing duplex (black). Data shown in (**C**) for A_2 (interstrand reaction) correspond with A_2-G separations of 5.0 Å (red) and 7.8 Å (blue) compared with an unquenched I-containing duplex (black). For A_ε, the quenching observed by steady-state emission spectroscopy is reflected as changes in the fluorescence decay profile (*23*) which can be satisfactorily described by a biexponential fit [G, 3.4 Å: τ_1 = 0.06 ns (70%), τ_2 = 2.0 ns (30%); G, 6.8 Å: τ_1 = 0.65 ns (75%), τ_2 = 6.9 ns (24%); I, 6.8 Å: τ_1 = 0.77 ns (73%), τ_2 = 7.3 ns (27%)]. Changes in decay lifetimes are also observed in the A_2-G duplexes [G, 3.4 Å: τ_1 = 1.9 ns (46%), τ_2 = 0.070 ns (54%); G, 6.8 Å: τ_1 = 1.3 ns (56%), τ_2 = 0.18 ns (44%); I, 6.8 Å: τ_1 = 3.1 ns (74%), τ_2 = 0.54 ns (26%)] but must be considered along with the large amounts of static quenching to account for all of the quenching observed in steady-state measurements (*27*). The interstrand quenching reaction between A_2 and G, in contrast to the mainly static quenching observed when the donor and acceptor were located on the same strand, is manifested as dynamic quenching. The decay profiles are complex, as both changes in lifetimes and percentages are observed, but can be fit to a biexponential decay [G, 5.0 Å: τ_1 = 1.8 ns (40%), τ_2 = 0.12 ns (60%); G, 7.8 Å: τ_1 = 1.8 ns (46%), τ_2 = 0.20 ns (54%); I, 7.8 Å: τ_1 = 2.2 ns (63%), τ_2 = 0.79 ns (37%)]. See (*40*) for further description of methods.

Steady-state emission spectroscopy, reflecting the extent of ET, revealed different behavior for the two fluorescent bases incorporated within DNA duplexes (Tables 1 and 2). Although both bases were highly quenched by G at the shortest donor-acceptor distance [F_q (3.4 Å): A_2 = 0.93(2), A_ε = 0.85(7)], only A_2 showed significant levels of ET quenching at larger separations [F_q (13.6 Å) = 0.21(1)]. Indeed, A_ε was only slightly reactive at 6.8 Å [F_q = 0.18(4)] and exhibited essentially no quenching at longer distances. Time-correlated single-photon counting (TCSPC) measurements furthermore revealed a difference in the rates of the G-dependent reaction for A_2 as compared with A_ε (Fig. 1, A and B). At 3.4 Å, where donor and acceptor are located at adjacent positions within the DNA helix, A_2 undergoes ET manifested as static quenching [a decrease in initial intensity, which indicates that the quenching reaction is faster than the time scale measured by this apparatus (100 ps) ($k_{ET} \geq 10^{10}\ s^{-1}$)]. In contrast, decreases in the measurable fluorescence lifetimes for A_ε completely account for the quenching of this base by G, indicating that ET takes place on a slower time scale ($k_{ET} \sim 10^9\ s^{-1}$) (*23*). Because the quenching of A_ε is dynamic, the distance dependence of the A_ε-G reaction provides a measure of β; on the basis of steady-state quantum yields, a value of 1.0(1) $Å^{-1}$ was obtained for this parameter (Fig. 2). Because the quenching reaction between A_2 and G occurs on a time scale faster than that predicted by a Stern-Volmer analysis, the distance dependence of this reaction calculated from steady-state quantum yields is not purely a reflection of β. The distance dependences of this and other ultrafast reactions must therefore be interpreted within the context of a different model (see below).

The reactivities toward GTP of A_2 and A_ε are essentially identical in solution. However, once incorporated into duplex DNA, there are striking differences. Fast ET initiated by photoexcited A_2 occurred over a range of distances, indicating that DNA provides strong coupling between reactants. A_ε exhibits slower ET with a steep distance dependence, indicating that DNA here acts as an insulator. High-resolution nuclear magnetic resonance (NMR) studies of duplexes containing A_2 (*24*) and A_ε (*25*) provide insight into a clear difference between these modified bases: stacking within the DNA helix. A_ε is sterically bulky, does not pair with T, and adopts a nonrigid, poorly stacked conformation within the base stack (*26*). A_2 undergoes normal Watson-Crick pairing with T and is stacked within the DNA helix quite similarly to the natural bases (*26*). The extent of stacking among these bases and the DNA base-pair stack affects the reaction kinetics and distance dependences of these ET processes mediated by the DNA helix. Indeed, subtle distinctions in stacking lead to large differences in reactivity. The very different distance dependences for these reactions may indicate that different pathways are accessed.

Base-base ET chemistry also provides an opportunity to examine coupling between donors and acceptors located on the same strand of DNA duplexes compared with that between reactants located on opposite strands (Fig. 3). Table 2 shows steady-state emission results for assemblies in which the interstrand reaction analogous to the intrastrand reaction described above was studied. Here, at the shortest distance studied for the interstrand reaction of A_2, 5.0 Å, 52(4)% of the emission intensity was quenched in a G-containing duplex. The yields of ET were again attenuated with increasing donor-acceptor separation but were much less sensitive to distance than for the intrastrand quenching reaction. Measurement of reaction kinetics by TCSPC revealed another important distinction between these reactions (Fig. 1C): The reaction kinetics were found to be significantly slower for the interstrand ET compared with the

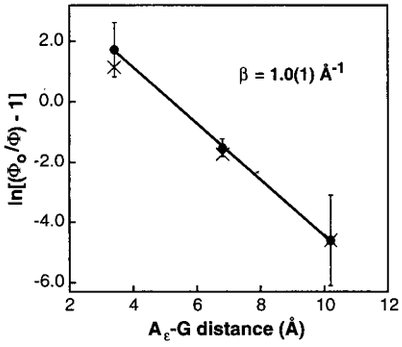

Fig. 2. Distance dependence of ET between A_ε and G. Steady-state quantum yields for unquenched (Φ_o), I-containing duplexes were compared with quenched (Φ), G-containing duplexes to evaluate the dependence of this reaction on distance. On the basis of the expressions $k_{et} = 1/[\tau_o(\Phi_o/\Phi) - 1]$ and $k_{et} = k_o e^{-\beta r}$, ($\tau_o$ = unquenched lifetime, r = distance in angstroms, k_o = rate of ET at r = 0), and the observation that the changes in quantum yield are reflected in the fluorescent decay lifetimes, the analysis of data in this manner yields an average value for β of 1.0(1) $Å^{-1}$. For comparison, data points obtained by quantitating quenching from the weight-averaged lifetimes determined in TCSPC experiments are also shown (indicated by crosses) (*23*). Although a discrete ET rate cannot be calculated because the fluorescence decay is multiexponential, the dependence of each component on distance is consistent with this value for β. Average lifetimes for unquenched samples were used for τ_o.

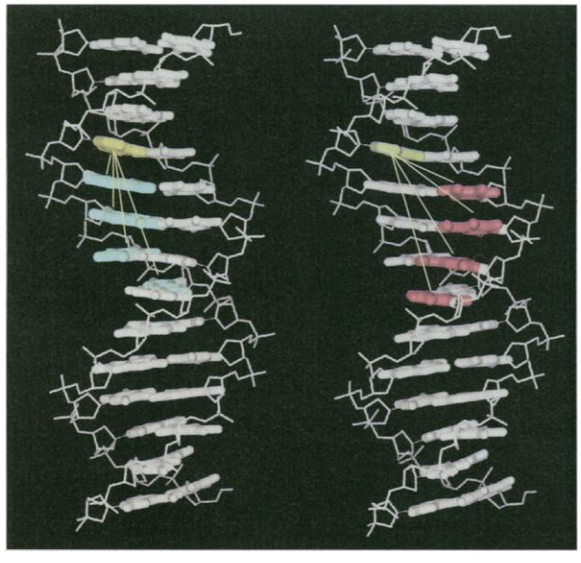

Fig. 3. Molecular models of A_2 assemblies used to evaluate intrastrand (left) and interstrand (right) quenching reactions of A_2 by G. Structures were minimized as described (*26*). The positions shown lead to donor-acceptor distances of 3.4, 6.8, 10.2, and 13.6 Å for the assemblies containing both donor and acceptor on the same strand, and A_2-G distances of 5.0, 7.8, 10.8, and 13.9 Å for duplexes with reactants located on opposite strands, if measured directly through space from the 2-NH_2 of A_2 to the 2-NH_2 of G.

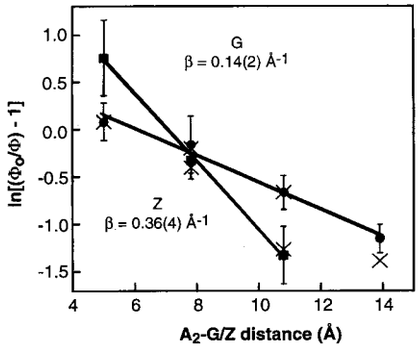

Fig. 4. Distance dependence of interstrand ET between A_2 and G (circles) or Z (squares). As the fluorescence quenching observed with donors and acceptors located on opposite strands on a DNA duplex are fully accounted for by changes in decay profiles, steady-state quenching yields can be evaluated as described in Fig. 2 to yield average values for β of 0.14(2) $Å^{-1}$ (A_2-G) and 0.36(4) $Å^{-1}$ (A_2-Z). For comparison, data points obtained by quantitating quenching from the weight-averaged lifetimes determined in TCSPC experiments are also shown (indicated by crosses) (*28*).

intrastrand reaction. Indeed, whereas a large proportion of the quenching is unresolvable with 100-ps resolution for the intrastrand reaction, the ET quenching for A_2 and G localized on different strands is completely resolved on the time scale observable in this experiment (*27*). Thus, ET is slower for the bases in this orientation. Because the distance dependence of the interstrand reaction results in measurable changes in ET rates, a value of 0.14(2) $Å^{-1}$ for β can be determined (Fig. 4).

Thus, ET proceeds preferentially down one strand in double-helical DNA. Within B-form DNA, essentially only intrastrand stacking occurs (*28*). When reactants are directly coupled through stacking along one strand, fast reaction kinetics result. If H-bonded base pairs must be traversed, the ET kinetics slow considerably. Nonetheless, a shallow distance dependence with $\beta = 0.1$ $Å^{-1}$ is observed. Comparably low values of β have been observed only for fully conjugated systems (*29*).

We also examined the effect of "cutting" a proximal interstrand connection by incorporating A_2 mispairs that lack H-bonding interactions. A_2 does not form a stable base pair with G; results of previous spectroscopic studies indicate a dynamic extrahelical conformation for the G of this pair (*30*, *31*). A comparison of quenching yields for the intrastrand and interstrand reactions for the Watson-Crick paired and mispaired fluorophore are depicted graphically in Fig. 5. Quenching yields for the intrastrand reaction decreased in the presence of an A_2-G mispair, but the overall distance dependence of the reaction was essentially identical to that observed with the A_2-T pair. However, for the interstrand reaction, the quenching yield decreased by ~50% at the shortest donor acceptor distance (5.0 Å), and the overall distance dependence is increased dramatically ($\beta \sim 1.7$ $Å^{-1}$). When the donor and acceptor are coupled through an intrastrand pathway, the direct stacking that facilitates the electronic interaction between the reactants appears to be only slightly perturbed by the mispair, leading to decreased yields of fast ET.

For donors and acceptors coupled through an interstrand pathway, H-bonding contacts between strands are essential for long-range reactivity, and thus, the overall distance dependence was sharply attenuated by the presence of an A_2 base pair with limited H bonding. The efficiency of the interstrand reaction at 5.0 Å was also measured in the presence of A_2-C and A_2-A pairs, and the quenching yields for these pairs [A_2-C: $F_q = 0.41(2)$, T_m(320 nm) = 25°C; A_2-A: $F_q = 0.54(3)$, T_m(320 nm) = 28°C] paralleled the strength of base-pairing interactions indicated by melting temperatures for the duplexes. These results implicate the H-bond–mediated interstrand connection between A_2 and its complementary thymine as an important component in the overall ET pathway for the interstrand reaction. The magnitude of the observed effect is somewhat surprising, as many other interstrand H bonds could potentially compensate for the disruption of the A_2 base pair; efficient interstrand reactions may require the excited state of A_2 to be directly coupled to the opposite strand (*32*).

The effect of driving force and reactant energetics on DNA-mediated ET has remained largely unexplored because of the difficulty of varying redox potentials without significantly changing the structure of synthetic assemblies. Base-base ET chemistry offers a means to examine this issue as well. Here, by simply substituting Z for G as the

Table 2. Steady-state quantum yields and quenching efficiencies for A_2-G/Z duplexes. Quantum yields (Φ) for 100 μM duplex samples in 100 mM phosphate (pH 7) were measured at 20°C relative to 100 μM A_2, $\Phi = 0.32$ (*12*). Samples were prepared as in (*39*). All solutions exhibited identical absorbances. Sample excitation was performed with $\lambda_{exc} = 325$ nm, and spectra were integrated from 340 to 500 nm. The emission spectra of quenched A_2-G samples displayed a more prominent emission shoulder at ~400 nm than other samples, likely because of a tautomeric form of A_2 with a lower energy excited state that could not react with G (*41*). Therefore, emission intensities were determined by monitoring emission at 360 nm, the maximum of the main peak, for a 60-s interval. Numbers in parentheses represent standard deviation values. The emission spectra of A_2-Z samples were distinctly sharper than others, again possibly because of a tautomeric form of A_2 with a lower energy excited state that is preferentially quenched. These spectral differences did not affect the quenching yields in this case more than 5%, and thus the entire spectrum was used.

Duplex	A_2-Y distance (Å)	$\Phi_{Y=I}$	$\Phi_{Y=G}$	F_q(G)	$\Phi_{Y=Z}$	F_q(Z)
		Intrastrand ET				
5′-TAI**A**YITITTATIA ATCTCCACAATACT	3.4	0.067 (3)	0.005 (1)	0.93 (2)	0.002 (1)	0.97 (2)
5′-TAI**A**AYITATTAIA ATCTTCCATAATCT	6.8	0.057 (4)	0.016 (2)	0.72 (2)	0.009 (1)	0.84 (4)
5′-TAI**A**AAYITITAIA ATCTTTCCACATCT	10.2	0.051 (4)	0.027 (3)	0.47 (4)	0.028 (5)	0.47 (6)
5′-TAI**A**AIAYITATIA ATCTTCTCCATACT	13.6	0.055 (4)	0.043 (8)	0.21 (1)	0.050 (4)	0.08 (4)
		Interstrand ET				
5′-TAI**A**CITITTATIA ATCT**Y**CACAATACT	5.0	0.052 (5)	0.025 (3)	0.52 (4)	0.017 (4)	0.68 (6)
5′-TAI**A**ACITATTAIA ATCTT**Y**CATAATCT	7.8	0.057 (3)	0.031 (3)	0.46 (5)	0.033 (3)	0.42 (5)
5′-TAI**A**AACITITAIA ATCTTT**Y**CACATCT	10.8	0.061 (3)	0.040 (4)	0.34 (2)	0.048 (4)	0.21 (3)
5′-TAI**A**AIACITATIA ATCTTCT**Y**CATACT	13.9	0.059 (7)	0.045 (6)	0.24 (2)	0.058 (5)	0.02 (4)

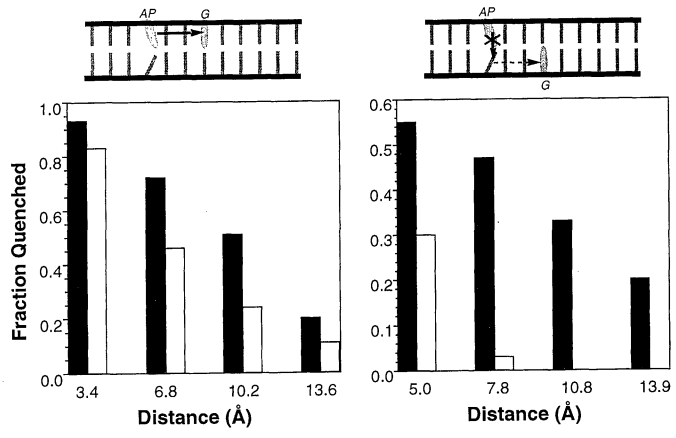

Fig. 5. Comparison of quenching yields for intrastrand (left) and interstrand (right) quenching between A_2 and G when A_2 is paired with T (black bars) or G (white bars). For the intrastrand quenching reaction, the mispairing of A_2 significantly decreases the ET efficiency but does not drastically affect the overall distance dependence. However, both the efficiency and distance dependence of the interstrand reaction are affected by the mispairing, with no quenching observed when the donor and acceptor were separated by more than two base pairs. It is therefore apparent that the H bonding between A_2 and its partner is critical for the propagation of long-range electronic coupling for reactions that involve donors and acceptors localized on different strands. Duplexes used in this experiment were analogous to those shown in Table 2, with the exception of G being substituted for T across from A_2. Melting temperatures for these mismatched duplexes were decreased by ~ 5°C relative to fully paired duplexes. The intensity of fluorescence for A_2 paired with G was 1.5 times that with T, consistent with a conformation of A_2 less well stacked within the helix.

electron donor in the A_2 assemblies (a change of one atom), the effect of lowering the oxidation potential of this reactant by ~300 mV can be monitored. In duplexes containing A_2 and Z either on the same or opposite strands, large amounts of fluorescence quenching were again observed (Table 2). The quenching yields at short distances were greater than for the analogous G-containing duplexes, consistent with the higher driving force for this reaction, but the overall distance dependences for the A_2-Z reactions were steeper. The kinetic profiles for the intrastrand versus interstrand Z reactions were generally analogous to those observed for the G reaction (*33*); hence, the distance dependence of the interstrand reaction yields another value of β in DNA. Here, for the interstrand A_2-Z reaction, $\beta = 0.36(4)$ Å^{-1} (Fig. 4).

The steeper distance dependence for the reaction of Z compared with G may confirm the importance of a parameter proposed in theoretical models for ET: tunneling energy (*34*). Because this DNA-mediated reaction, and most of the others studied to date, use reactants with potentials close to those of the DNA bridge (*4, 5, 8–10*), a mechanism may be operative where the energetic gap between reactant orbitals and bridge orbitals (referred to as tunneling energy) becomes a crucial factor modulating the distance dependence of ET. Recent studies of ET in synthetic conjugated oligomers have provided evidence for enhanced electronic coupling with small tunneling energies (*35*). Indeed, by decreasing the donor oxidation potential here, we might be able to increase the energetic gap between this reactant and the bridge (*36*).

Reactant energetics clearly modulate the distance dependence of ET in DNA, but these effects cannot completely explain the broad range of results obtained in systems with different reactants. Many of the photoexcited acceptors used in different studies react selectively with G, indicating that these reactions have similar tunneling energies, yet markedly different distance dependences are observed ($\beta \sim 0.6$ to 1.4 Å^{-1}) (*8, 10*). Moreover, the reactions of ethidium with Z or intercalators that have larger tunneling energies also have shallow distance dependences ($\beta \leq 0.1$ to 0.4 Å^{-1}) (*4, 5*). We observed distance dependences differing by an order of magnitude for the reactions of A_2 and A_ε, which have excited-state energies differing by no more that 100 mV. Therefore, although tunneling energies may somewhat modulate the efficiency of ET through DNA, the strong stacking interactions between reactants and the DNA bases that are present in all of the systems with shallow distance dependences must also be essential.

Table 3 summarizes the distance dependences for base-base ET reactions described here as well as our interpretations of these data. The very fast intrastrand reactions of A_2 with G or Z resemble those observed with intercalating reactants (*4, 5*). Static quenching, indicative of ET with rates $\geq 10^{10}$ s^{-1}, dominates these reactions at all donor-acceptor distances. Hence, the attenuation of quenching yields as a function of distance does not appear to reflect only a competition between the rate of ET and the excited-state decay. We have previously proposed that base and reactant dynamics may effectively "gate" the yields of these reactions, thereby influencing the overall distance dependence because more intervening base pairs would result in a higher probability of a destacked duplex. Internal motions have been detected within DNA on picosecond time scales (*37*). Therefore, if ET were to occur on this time scale or faster, only molecules in a limited range of conformations leading to the strong coupling required for this fast reaction may be active. The distance dependences for the A_2-G and A_2-Z intrastrand reactions (Fig. 6) do not provide true measures of β because of the extent of static quenching at all donor-acceptor distances despite decreasing ET yields. We represent these distance dependences as γ, which is a measure of the exponential dependence of ET yield, rather than rate, on distance. These values, $\gamma = 0.38(3)$ Å^{-1} for A_2-G and $\gamma = 0.59(2)$ Å^{-1} for A_2-Z, may represent upper limits for β. The observation of steeper distance dependences for the fast intrastrand reactions compared with the slower interstrand reactions is consistent with the proposal that base destacking dynamics limit the efficiency of the faster reactions and contribute to the overall distance dependence. Interestingly, the distance dependences for the intrastrand reactions of A_2 with G as compared with Z also show a sensitivity to reactant energetics.

The distance dependences of the intrastrand A_2-G and A_2-Z reactions can be directly compared with those measured previously for the oxidative quenching of ethidium by a rhodium intercalator (*4*), where $\gamma = 0.1$ Å^{-1}, and the photooxidation of Z by ethidium (*5*), where values for γ from 0.2 to 0.4 Å^{-1} were measured (Fig. 6). This range of distance dependences for these fast reactions, where γ(intercalator/intercalator) < γ(intercalator/base) < γ(base/base), appears to reflect the different extents of interaction between these reactants with the DNA base stack, contributing either to stronger coupling between reactants, or higher reaction probabilities. ET on fast time scales occurring over significant distances is a general phenomenon that can be observed when intercalators and modified bases are used as reactants.

Our data clearly show that (i) strong reactant stacking is essential for fast long-range ET through DNA, (ii) ET proceeds preferen-

Table 3. Summary of distance dependences for base-base ET reactions. Dashes indicate not applicable.

Reaction	Acceptor	Donor	Distance dependence		Conclusions
			β	γ	
Intrastrand	A_ε	G	1.0 Å^{-1}	—	Weak coupling $k_{ET} < k_{base\ dynamics}$
Intrastrand	A_2	G	—	0.4 Å^{-1}	Direct coupling
Intrastrand	A_2	Z	—	0.6 Å^{-1}	$k_{ET} \geq k_{base\ dynamics}$
Interstrand	A_2	G	0.1 Å^{-1}	—	Indirect coupling
Interstrand	A_2	Z	0.4 Å^{-1}	—	$k_{ET} < k_{base\ dynamics}$

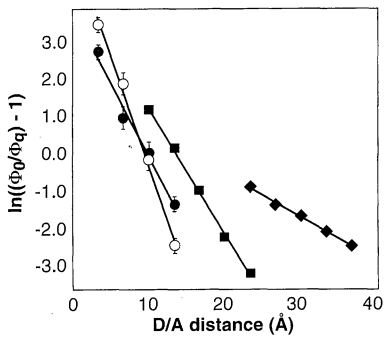

Fig. 6. Distance dependences (γ) for intrastrand reactions between A_2 and G (closed circles) or Z (open circles). As quenching reactions for donors and acceptors localized on the same strand include significant contributions from fast static quenching, the distance dependence of these processes, just as those previously measured for oxidative quenching of ethidium by $Rh(phi)_2bpy^{3+}$ and the photooxidation of Z by ethidium, are not direct measurements of β. These distance dependences instead represent lower limits for this parameter and include differing effects of stacking probabilities for reactants and the intervening DNA bases. The reaction between two intercalators has the most shallow distance dependence (closed diamonds, $\gamma = 0.1$ Å^{-1}), followed by the reaction between one intercalator and a modified base (closed squares, $\gamma = 0.4$ Å^{-1}), with reactions between two bases exhibiting the steepest distance dependences [A_2-G, $\gamma = 0.38(3)$ Å^{-1}; A_2-Z, $\gamma = 0.59(2)$ Å^{-1}]. These results indicate that the reactants interacting with the base stack with larger surface areas may be more strongly coupled into the stack, possibly because of slower exchange dynamics.

tially through directly stacked intrastrand pathways compared with interstrand pathways, and (iii) the distance dependence of ET in DNA varies with donor energy. We can conclude that a coherent, well-stacked pathway within the DNA helix is associated with an extremely low value of β, 0.1 $Å^{-1}$. Values of β approaching 1.0 $Å^{-1}$ are associated with pathways not directly coupled through strong stacking interactions, and it is not clear in those cases whether the pathway is even mediated by the base pairs. The empirical observation of low values of β in well-stacked DNA does not imply a mechanism, however. Certainly theoretical descriptions of ET in weakly coupled systems are insufficient to describe the DNA bridge with such a low value of β, and the sensitivity of β to donor energies suggests that this ET reaction may be better described within the adiabatic regime (*38*). Although hopping mechanisms may account at least in part for the longer range chemistry observed in our laboratory and elsewhere (*2, 9*), where a shallow distance dependence is observed by monitoring emission from the excited-state acceptor, other direct coupling mechanisms may need to be invoked.

Here, a range of reactivity was observed in analogous DNA assemblies with exponential distance dependences for ET spanning a full order of magnitude. The range of results we obtained with reactants so similar, or even identical in structure but not in stacking orientation, suggests that the various results found with different types of reactants can be understood in terms of sensitivity to stacking, orientation, and energetics (*3–10*). The assessment of DNA as a medium for ET cannot be made simply from measurements of the effect of distance, but also requires the consideration of parameters that are unique to this π-stacked molecular assembly. Paradigms developed to describe long-range ET in σ-bonded systems such as proteins cannot be simply applied to describe the exquisite sensitivity of charge transport in DNA to π-stacking interactions and energetics.

References and Notes

1. R. E. Holmlin, P. J. Dandliker, J. K. Barton, *Angew. Chem. Int. Ed.* **36**, 2714 (1997); S. O. Kelley and J. K. Barton, *Met. Ions Biol. Sys.*, in press.
2. D. B. Hall, R. E. Holmlin, J. K. Barton, *Nature* **382**, 731 (1996); D. B. Hall and J. K. Barton, *J. Am. Chem. Soc.* **119**, 5045 (1997); M. R. Arkin, E. D. A. Stemp, J. K. Barton, *Chem. Biol.* **4**, 389 (1997); P. J. Dandliker, R. E. Holmlin, J. K. Barton, *Science* **275**, 1465 (1997); S. M. Gasper and G. B. Schuster, *J. Am. Chem. Soc.* **119**, 12762 (1997); P. J. Dandliker, M. E. Nunez, J. K. Barton, *Biochemistry* **37**, 6491 (1998).
3. C. J. Murphy *et al.*, *Science* **262**, 1025 (1993); C. J. Murphy *et al.*, *Proc. Natl. Acad. Sci. U.S.A.* **91**, 5315 (1994); M. R. Arkin *et al.*, *Science* **273**, 475 (1996).
4. S. O. Kelley, R. E. Holmlin, E. D. A. Stemp, J. K. Barton, *J. Am. Chem. Soc.* **119**, 9861 (1997).
5. S. O. Kelley and J. K. Barton, *Chem. Biol.* **8**, 413 (1997).
6. S. O. Kelley, N. M. Jackson, M. G. Hill, J. K. Barton, *Angew. Chem. Int. Ed.*, in press.
7. T. J. Meade and J. F. Kayyem, *Angew. Chem. Int. Ed.* **34**, 352 (1995).
8. F. D. Lewis *et al.*, *Science* **277**, 673 (1997); F. D. Lewis and R. L. Letsinger, *J. Bioinorg. Chem.* **3**, 215 (1998).
9. E. Meggers, D. Kusch, M. Spichty, U. Wille, B. Giese, *Angew. Chem. Int. Ed.* **37**, 460 (1998).
10. K. Fukui and K. Tanaka, *ibid.*, p. 158.
11. R. A. Marcus and N. Sutin, *Biochim. Biophys. Acta* **811**, 265 (1985).
12. D. C. Ward, E. Reich, L. Stryer, *J. Biol. Chem.* **244**, 1228 (1969).
13. J. R. Barrio, J. A. Secrist, N. J. Leonard, *Biochem. Biophys. Res. Commun.* **46**, 597 (1972); J. A. Secrist, J. R. Barrio, N. J. Leonard, G. Weber, *Biochemistry* **11**, 3499 (1972); R. D. Spencer, G. Weber, G. L. Tolman, J. R. Barrio, N. J. Leonard, *Eur. J. Biochem.* **45**, 425 (1974).
14. A. Holmen, B. Norden, B. Albinsson, *J. Am. Chem. Soc.* **119**, 3114 (1997); A. Broo, *J. Phys. Chem. A* **102**, 526 (1998).
15. A. Holmen, B. Norden, B. Albinsson, *J. Phys. Chem.* **98**, 13460 (1994).
16. The potentials of G, Z; and I are ~ +1.3 V, +1.0 V, and +1.5 V versus NHE, respectively (*5*).
17. C. A. M. Seidel, A. Schultz, M. H. M. Sauer, *J. Phys. Chem.* **100**, 5541 (1996); S. Steenken and S. V. Jovanovic, *J. Am. Chem. Soc.* **119**, 617 (1997).
18. The equally low levels of quenching observed with deoxyinosine triphosphate, deoxyadenosine triphosphate, deoxycytidine triphosphate, and deoxythymidine triphosphate were not sensitive to the redox potentials of these bases (*17*), and therefore do not appear to be the result of ET.
19. In these titrations, the A_2 free base and A_ε nucleotide triphosphate were used. For the nucleotide triphosphate form of A_2, smaller k_q values would be expected as a result of higher electrostatic repulsions with the nucleotide triphosphate quenchers and an increase in the reduction potential of the alkylated base.
20. Upon flash photolysis of solutions containing 100 μM A_2 and 50 mM dGTP, long-lived signals were observed on the microsecond time scale by transient absorption with spectral characteristics (maximum wavelength λ_{max} = 310 nm, 380 nm, 550 nm) consistent with the well-characterized neutral G radical [L. P. Candeias and S. Steenken, *J. Am. Chem. Soc.* **111**, 1094 (1989); E. D. A. Stemp, M. R. Arkin, J. K. Barton, *ibid.* **119**, 2921 (1997)]. Similar results were obtained with A_ε.
21. Using excited-state energies approximated from intersection points of absorption and emission spectra (E_{oo}) and electrochemical potentials [$E°(^{o}/^{-})$], we calculated the excited state reduction potentials of A_2 and A_ε from the expression $E°(^{*}/^{-}) = E_{oo} - E°(^{o}/^{-})$ as +1.5 and +1.4 V versus NHE, respectively.
22. Because the fluorescence of A_2 is sensitive to its environment within the base stack, the quantum yields of unquenched I-containing duplexes were carefully monitored to delineate the effect of the subtle variations in sequence in the duplexes (Table 2). The first duplex of the series consistently exhibited a higher quantum yield than the others of this series, presumably because of poorer stacking of A_2 with I. However, throughout the rest of the series, constant quantum yields were obtained, indicating that (i) the environment of A_2 is essentially identical, and (ii) I-dependent reactions were not occurring.
23. Because the decays of A_ε are multiexponential, as expected for a DNA-bound probe, the fits of the fluorescence decay profiles do not yield single rate constants for the ET reaction between A_ε and G. However, the integration of the decay curves for the G-containing and I-containing duplexes provides a measure of dynamic quenching that is independent of any data-fitting routine. These quenching yields are identical to those observed in steady-state measurements, allowing the calculation of β. An analysis of the fluorescence decay data is available www.sciencemag.org/feature/data/984892.shl as supplementary material.
24. M. Kouchakdijan *et al.*, *Biochemistry* **30**, 1820 (1991).
25. T.M. Norlund *et al.*, *ibid.* **28**, 9095 (1989).
26. It is well established that A_ε assumes a nonplanar orientation within the helix and is poorly stacked with the other DNA bases (*24*). In addition, force-field calculations on A_ε-containing duplexes also reveal significant perturbations in stacking at the site of this modified base (see below). These features of the conformation of A_ε are consistent with physical and photophysical characteristics of the duplexes we prepared containing this base. Significant decreases (~5°C) in the thermal denaturation temperatures are observed for duplexes containing A_ε compared with adenine, and no hypochromism or transitions upon thermal denaturation in the 310-nm absorption associated with A_ε is detected. Moreover, very low steady-state fluorescence polarization values (~0.01) were observed for A_ε duplexes. We found that A_2 exhibits much higher levels of steady-state polarization (~0.15) and a smaller destabilizing effect on duplex stability (1° to 2°C) compared with A_ε. Furthermore, thermal denaturation of A_2-containing duplexes can be monitored in the 310-nm absorption unique to this base, because it is red-shifted when this base is within a hybridized duplex. This change may result from a more nonpolar environment for the base, or as the result of H-bonding interactions. Thermal denaturation transitions can therefore be monitored at this wavelength and are observed to occur 2° to 3°C before the transitions monitored at 260 nm corresponding to the melting of the entire duplex. Duplexes containing either A_ε or A_2 were constructed with commercial software (Macromodel) and minimized with the AMBER force field. These calculations revealed structures for the duplexes consistent with those obtained from NMR studies (*24, 25*), with a nonplanar, poorly stacked orientation for A_ε incorporated across from T within the DNA helix. In contrast, A_2-T pairs were essentially indistinguishable from A-T pairs.
27. The fluorescence decay kinetics for A_2 are also multiexponential. For the interstrand A_2-G reaction, good agreement is obtained between the dynamic quenching quantitated from TCSPC and the total quenching observed using steady-state methods, hence steady-state quantum yields can be utilized for the calculation of β. The same agreement is not observed for the intrastrand A_2-G reaction because of the significant amount of static quenching, and therefore, the dependence of these quenching yields on distance does not solely reflect β. An analysis of the fluorescence decay data is available www.sciencemag.org/feature/data/984892.shl as supplementary material.
28. W. Saenger, *Principles of Nucleic Acid Structure* (Springer-Verlag, New York, 1984).
29. S. Woitellier, J. P. Launay, C. W. Spangler, *Inorg. Chem.* **28**, 758 (1989).
30. C. R. Guest, R. A Hochstrasser, L. C. Sowers, D. P. Millar, *Biochemistry* **30**, 3271 (1991).
31. Within the A_2-G-mispair–containing duplexes, the A_2 310-nm absorption is not red-shifted. Furthermore, although the overall melting of the A_2-G duplex can be observed at 260 nm [melting temperature T_m(260 nm) = 24°C (A_2-G); T_m = 30°C (A_2-T)], no transition can be detected in the A_2 absorption. It therefore appears that A_2 is neither H-bonded nor well stacked within the A_2-G mispair, consistent with photophysical studies (*29*). Furthermore, almost twofold increases are observed for the steady-state quantum yields of A_2-G duplexes compared with those with Watson-Crick pairs, again indicating that the fluorophore is not well stacked within the duplex. The high quantum yields observed in these samples also indicate that G and A_2 do not participate in efficient ET when incorporated within a mispair and therefore do not interact strongly.
32. Consistent with these observations, A_ε (which is not H bonded when incorporated across from T) shows only very small amounts of interstrand quenching with G (<10%) 5.0 Å away.
33. For the ET between A_2 and Z, large amounts of static quenching are again observed for the intrastrand reaction, but full resolution of the quenching kinetics is achieved for the interstrand reaction with ~100-ps resolution. Although the decay profiles are complex, it is evident from these data that the kinetics of ET for the interstrand A_2/Z reaction are faster than

those of the analogous A_2/G reaction, as expected for the higher driving force reaction.
34. J. W. Evenson and M. Karplus, *Science* **262**, 1247 (1993); S. Priyadarshy, S. M. Risser, D. N. Beratan, *J. Bioinorg. Chem.* **3**, 196 (1998); J. J. Regan *et al.*, *Chem. Biol.* **2**, 489 (1995).
35. W. B. Davis, W. A. Svec, M. A. Ratner, M. R. Wasielewski, *Nature* **396**, 60 (1998).
36. Alternatively, the nitrogen-to-carbon substitution in Z compared with the natural base may decrease the strength of stacking interactions for this modified base. However, the use of deazaadenine (which has an oxidation potential quite similar to that of G) as an electron donor in analogous experiments produced an interstrand distance dependence almost identical to that observed with G (S. O. Kelly and J. K. Barton, data not shown). Therefore, it appears that the increased distance dependence for the A_2-Z reaction results from energetic effects.
37. S. Georghiou, T. D Bradrick, A. Philippetis, J. M. Beechem, *Biophys. J.* **70**, 1909 (1996).
38. J. Jortner, M. Bixon, T. Langenbacher, M. E. Michel-Beyerle, *Proc. Natl. Acad. Sci. U.S.A.* **95**, 12759 (1998); A. K. Felts, W. T. Pollard, R. A. Freisner, *J. Phys. Chem.* **99**, 2929 (1995); A. Okada, V. Chernyak, S. Mukamel, *idib.* **102**, 1241 (1998).
39. A_e, A_2, I, and Z phosphoramidites were all obtained from Glen Research. Oligonucleotides were prepared by standard automated techniques (with the exceptions described below) on a 394 ABI synthesizer and purified by reverse phase high-performance liquid chromatography. For Z, the oxidation step was carried out with 10-camphorsulfonyl oxaziridine as previously described (*5*). Base deprotection of ethenoadenine-containing oligonucleotides was carried out for 24 hours at room temperature. Oligonucleotides containing modified bases were characterized by electrospray mass spectroscopy. Samples were prepared as follows: on the basis of the calculated extinction coefficients for DNA sequences [ε_{260} (M^{-1} cm^{-1}): dC = 7.4×10^3; dG = 12.3×10^3; dT = 6.7×10^3; dA = 15.0×10^3; dZ-G = 10.5×10^3; dI = 11.0×10^3 ; d(A_e) = 4.5×10^3; d(A_2) = 2.5×10^3], appropriate amounts of complementary materials were combined at 1:1 stoichiometry and dissolved in 100 mM sodium phosphate (pH 7) to give a final duplex concentration of 100 μM. The resulting solutions were heated to 90°C and slowly cooled to ambient temperature over 2 to 3 hours to anneal the duplex. The ultraviolet-visible spectra of the duplex samples were carefully measured to ensure that the absorbance at the excitation wavelength was identical for every sample. Thermal denaturation experiments were performed on a HP8452A diode array spectrophotometer with samples at a duplex concentration of 25 μM in 100 mM phosphate (pH 7). Absorbance was monitored every 2°C with 3-min equilibration times. All duplexes used in these experiments exhibited cooperative thermal denaturation profiles with melting temperatures >25°C with 25 μM duplex and therefore were fully hybridized under the conditions of all fluorescence experiments (100 μM, 20°C).
40. Measurements were performed on a TCSPC apparatus previously described (*4*). Excitation was performed at 325 nm, and emission was monitored at 350 nm for A_2 and 400 nm for A_e. Two data sets were obtained for each sample, one containing >10,000 counts for the determination of decay lifetimes, and another taken over a 120-s time interval to quantitate static quenching. Experiments were otherwise performed under the same conditions as steady-state experiments (100 μM duplex, 100 mM sodium phosphate, pH 7).
41. C. Santhosh and P. C. Mishra, *Spectrochim. Acta* **47A**, 1685 (1991).
42. We thank E. Stemp for assistance with transient absorption experiments, R. Villahermosa for assistance with single-photon counting measurements, and T. Fiebig for discussions and assistance with molecular modeling. In addition, we acknowledge the NIH (grant GM49216 to J.K.B., predoctoral traineeship to S.O.K.) for financial support.

27 August 1998; accepted 7 December 1998

Emergent Properties of Networks of Biological Signaling Pathways

Upinder S. Bhalla and Ravi Iyengar*

Many distinct signaling pathways allow the cell to receive, process, and respond to information. Often, components of different pathways interact, resulting in signaling networks. Biochemical signaling networks were constructed with experimentally obtained constants and analyzed by computational methods to understand their role in complex biological processes. These networks exhibit emergent properties such as integration of signals across multiple time scales, generation of distinct outputs depending on input strength and duration, and self-sustaining feedback loops. Feedback can result in bistable behavior with discrete steady-state activities, well-defined input thresholds for transition between states and prolonged signal output, and signal modulation in response to transient stimuli. These properties of signaling networks raise the possibility that information for "learned behavior" of biological systems may be stored within intracellular biochemical reactions that comprise signaling pathways.

Studies on the cyclic adenosine monophosphate (cAMP) signaling pathway led to the identification of several general mechanisms of signal transfer, such as regulation by protein-protein interactions, protein phosphorylation, regulation of enzymatic activity, production of second messengers, and cell surface signal transduction systems (*1*). These mechanisms of signal transfer have subsequently been shown to occur in many pathways, including Ca^{2+} signaling pathways (*2*), tyrosine kinase pathways (*3*), and other protein kinase cascades, and recently in the intracellular protease cascades in apoptosis (*4*). Initially, signaling pathways were studied in a linear fashion, and it was shown that many important biological effects are obtained through linear information transfer. However, it has become increasingly clear that signaling pathways interact with one another and the final biological response is shaped by interaction between pathways. These interactions result in networks that are quite complex and may have properties that are nonintuitive. A systematic analysis of interactions between signaling pathways could be useful in understanding the properties of these networks. We developed models for simple networks consisting of up to four signaling pathways to determine if the network has properties that the individual pathways do not and if networking results in persistent activation of protein kinases after transient stimulus. Persistent activation of protein kinases is a general mechanism for eliciting biological effects. Cholera toxin continuously elevates cAMP, resulting in persistent activation of protein kinase A (PKA), inhibition of intestinal water reabsorption, and diarrhea, key pathological manifestations of cholera (*5*). Since this original demonstration, persistent activation of protein kinases has been implicated in diverse processes such as neoplastic transformation (*6*) and learning and memory (*7*). Although mutations or altered gene expression can result in persistent activation of protein kinases, we wished to ask the following question: Do connections between preexisting signaling pathways result in persistently activated protein kinases capable of eliciting end-point biological effects?

To develop models of signaling pathways, it is necessary to consider the mechanisms by which signal transfer occurs. In biological systems, signal transmission occurs mostly through two mechanisms: (i) protein-protein interactions and enzymatic reactions such as protein phosphorylation and dephosphorylation (ii) or protein degradation or production of intracellular messengers. In an approach that would include all of these reactions, we used the basic chemical reaction schemes of

$$A + B \underset{k_b}{\overset{k_f}{\rightleftharpoons}} AB \quad (1)$$

$$A + B \underset{k_b}{\overset{k_f}{\rightleftharpoons}} C + D \quad (2)$$

U. S. Bhalla, Department of Pharmacology, Mount Sinai School of Medicine, New York, NY 10029, USA, and National Centre for Biological Sciences, Post Office Box 1234, Bangalore 560012, India. R. Iyengar, Department of Pharmacology, Mount Sinai School of Medicine, New York, NY 10029, USA.

*To whom correspondence should be addressed.